Ultrahigh-pressure metamorphism in the magnesite + aragonite stability field: evidence from two impure marbles from the Dabie-Sulu UHPM belt.

Proyer A., Rolfo F., Zhu Y.F., Castelli D., Compagnoni R.
Ultrahigh-pressure metamorphism in the magnesite + aragonite stability field: evidence from two impure marbles from the Dabie-Sulu UHPM belt.
JOURNAL OF METAMORPHIC GEOLOGY (2013) 31
DOI: 10.1111/jmg.12005

Ultrahigh-pressure metamorphism in the magnesite + aragonite stability field: evidence from two impure marbles from the Dabie-Sulu UHPM belt.

ALEXANDER PROYER[1*], FRANCO ROLFO[2], YONG-FENG ZHU[3], DANIELE CASTELLI[2], ROBERTO COMPAGNONI[2]

[1] University of Graz, Universitaetsplatz 2/II, 8010 Graz, Austria;

*Corresponding author, e-mail: alexander.proyer@uni-graz.at

[2]University of Torino, Via Valperga Caluso 35,10135 Torino, Italy

[3]Peking University, Beijing 100871, China

Short title: UHPM in the magnesite + aragonite stability field

ABSTRACT

Two magnesite-bearing impure dolomitic marbles from the Dabie-Sulu UHP region have been investigated in order to clarify if they had actually attained *P-T* conditions outside the dolomite stability field, limited by the reaction dolomite = aragonite + magnesite, and to test their potential for recording (U)HP conditions. In both cases the silicate mineral assemblage records conditions around the terminal amphibole breakdown reaction: amphibole + aragonite ± quartz = clinopyroxene + talc, which is a good geobarometer between at least 2.0 and 2.6 GPa. At higher pressures, the terminal breakdown of talc to clinopyroxene + coesite is another *P-T* milestone that can be inferred from possible pseudomorphs of talc + calcite after coesite, at least in one sample. The dolomite dissociation curve becomes strongly divariant in Fe-bearing marbles and may be attainable during cold subduction near the 5°C/km "geotherm". At least one of the samples (from Xinyan village, near Taihu, Dabie Shan) preserved relics of both magnesite and aragonite and most likely attained conditions within the aragonite + magnesite stability field. For the second sample from Sanqingge village in the Sulu terrane no certain evidence has been found in this study. Impure dolomitic marbles have considerable potential to preserve (ultra)high-pressure relics, and the inconspicuous mineral assemblage clinopyroxene + talc or quartz (after former coesite) may in fact record UHP conditions.

Keywords: UHP metamorphism, dolomite dissociation, magnesite, aragonite, Dabie-Sulu

INTRODUCTION

The mineral assemblage magnesite + aragonite is of considerable interest for researchers dealing with ultrahigh-pressure (UHP) metamorphism, crust-mantle interaction or carbonate stability in the upper mantle because the breakdown of dolomite to magnesite + aragonite has been determined in a series of experiments (Liu & Lin, 1995; Martinez *et al.,* 1996; Luth, 2001; Sato & Katsura, 2001; Buob *et al.,* 2006; Morlidge *et al.,* 2006) to occur at very high pressures, within the so-called "forbidden zone", i.e. at "geothermal gradients" below 5°C per km (Fig. 1). Even though there is a considerable spread between the different experimental results, search for traces indicating the (former) presence of a magnesite + aragonite bearing mineral assemblage in ultrahigh-pressure marbles or eclogites is indicated because the number of possible geothermobarometers in that *P-T* range is very limited and the tectonic consequences of such finds quite important.

Although dolomitic marbles can be found in almost any UHP metamorphic area with metamorphosed supracrustal rocks, only Zhu & Ogasawara (2002) and Zhu (2005) reported observation of dolomite decomposition in marbles from Kokchetav and from the Sulu-terrane in China, but these observations were contested (Hermann, 2003; Zhu, 2003) or revised after a more detailed investigation (Zhu *et al.,* 2009) to the effect that the dolomite-magnesite marble investigated had not crossed the dolomite-out curve. Omori *et al.* (1999) discovered rare magnesite in impure dolomitic marbles from Xinyan (Dabie Shan) and concluded from the apparent textural disequilibrium of calcite-magnesite intergrowths that this rock also had not experienced pressures above the dolomite dissociation curve. Liu *et al.* (2006) however claim from inclusions of both aragonite and magnesite in the same "UHP growth zone" in

zircon that these marbles had passed the dolomite-out curve during their metamorphic history.

Carbonate-bearing eclogites and metapelites from Dabie Shan and Tian Shan in China however are reported to fulfill the requirements: Zhang & Liou (1996) describe a dolomite-magnesite-bearing coesite-eclogite that also contains calcite-pseudomorphs after former aragonite as inclusions in garnet, and Zhang *et al.* (2003) observed inclusions of magnesite and calcite (interpreted as pseudomorphs after former aragonite) in large dolomite porphyroblasts in a garnet-chloritoid-glaucophane micaschist. In both cases, a former coexistence of magnesite and aragonite was inferred. Only one carbonate mineral is stable at a time, however, in the majority of carbonate-bearing metabasites, with a reported change with increasing pressure from aragonite to dolomite to magnesite-bearing blueschists and eclogites (e.g. Messiga *et al.,* 1999; Zhang *et al.,* 2003).

The present study is a detailed investigation of magnesite-bearing dolomitic marbles sampled from the same localities as those of Omori *et al.* (1999) and Zhu *et al.* (2009) with the purpose of understanding the complex calcite-dolomite-magnesite intergrowth microstructures in order to establish whether the dolomite dissociation curve had actually been overstepped at some point of the metamorphic history of these rocks.

SAMPLE LOCATIONS

The first sample of impure dolomitic marble (RPC-159) was taken from a river profile near Xinyan, less than 2 km from the well known Shima gneiss+eclogite and Maowu garnet-peridotite in the Coesite Eclogite Complex of eastern Dabie Shan. The local geology,

lithologies and metamorphic history as derived mainly from eclogites have been described in Zhang & Liou (1996), Omori *et al.* (1999), Oberhänsli *et al.* (2002), Schmid *et al.* (2000, 2003) and Rolfo *et al.* (2004) and will not be covered here.

The second sample (XU-1) was collected in a quarry ca. 1 km northeast of the village of Sanqingge in the Sulu terrane. The location and its geological inventory are described in detail in Zhu *et al.* (2009). Folded bands of mostly dolomitic marble are separated by thin layers of eclogite, and three different types of marble, depending on the degree of retrogression, have been distinguished (Zhu *et al.,* 2009). The sample used for this study belongs to the least retrogressed magnesite marble type and was taken directly from the contact with an eclogite layer.

PETROGRAPHY

Sample RPC-159

This is a dolomite marble that contains large porphyroblasts of omphacite and tremolite (Fig. 2a) together with subordinate calcite and the accessory minerals epidote, zircon, rutile, apatite, pyrrhotite and chalcopyrite. Quartz is found only as inclusions in tremolite or at grain boundaries between tremolite and omphacite, magnesite as inclusions in dolomite and tiny relics of talc are rarely preserved in matrix dolomite (Fig. 2b). Omphacite and tremolite porphyroblasts are xenomorphic, with no apparent compositional zoning in spite of their large grain sizes of up to several millimeters. Epidote can be found both as inclusions and in the rock matrix and shows oscillatory zoning with local enrichment in Ce and Fe^{3+} (Fig. 2c). The degree of retrogression is minor: omphacite decomposes into a fine- to medium-grained symplectite of diopside + tremolite + albite ± calcite (Fig. 2d). Rutile affected by such alteration zones is partly replaced by titanite (Fig. 2e). The symplectites around phengitic

muscovite consist of Ba-rich muscovite + phlogopite + albite (Fig. 2f). Rounded inclusions of microcrystalline talc + calcite in omphacite, surrounded by cracks could be pseudomorphs after former coesite (Fig. 2g). Apatite cores are strewn with micrometer-sized blebs and needles of a Ce-rich phosphate – presumably monazite. The needles are crystallographically oriented in at least three different directions, indicating a precipitate origin (Fig. 2h).

The most revelatory mineral microstructures are those of the carbonate phases. Magnesite has yet been found only as inclusions in dolomite, but its degree of preservation can vary from completely fresh, often oval grains with straight grain boundaries to completely replaced by a porous type of calcite with or without additional dolomite or a Mg-Si-bearing talc-like mineral, which is, however, too poorly crystallized for a reasonable microprobe measurement. The various states of replacement are documented in Figs 3a-d.

Calcite occurs in three different morphological varieties. Pseudomorphic replacement of magnesite invariably results in a porous type of calcite (Fig. 3d). Another type of matrix calcite contains abundant blebs of dolomite and is interpreted as former high-Mg-calcite (Fig. 3e). Some, but not all of these calcite grains are found as part of medium grained amphibole + quartz or symplectite replacement microstructures after omphacite, and could be by-products of the omphacite breakdown reaction. A third type of calcite is devoid of pores and of dolomite inclusions. It was observed mainly as inclusions in omphacite, often with concentric cracks, and more rarely included in dolomite or adjacent to omphacite or dolomite grains (Figs 3f,g). One such grain contains relics of a BSE-brighter $CaCO_3$ mineral, which is aragonite (Fig. 3g), as verified by Raman spectra which show a peak at 206 wavenumbers which is typical for aragonite and absent in calcite. The Mg-content of the latter calcites is negligible (see below), consequently these grains are considered to represent former aragonite

as well. Finally, BSE-imaging revealed dolomite within dolomite, i.e. a grain of dolomite with a brighter BSE-contrast than the surrounding "normal" matrix dolomite (Fig. 3h).

Sample XU-1

The thin section of sample XU-1 goes right across the contact between eclogite and dolomitic marble, which are separated by a thin monomineralic band of amphibole 2-3 mm across. The eclogite consists mainly of omphacite and subordinate garnet, phengite and rutile, which are rimmed or replaced respectively by: symplectites of amphibole + plagioclase, Fe-Al-rich amphibole, symplectites of biotite + plagioclase, and titanite. The marble is composed of dolomite, calcite, amphibole, talc and very minor chlorite (Fig. 4a). Both tremolite and talc are coarse-grained (up to mm-sized). Talc is inclusion-free whereas tremolite often contains inclusions of quartz and more rarely of omphacite, magnesite and calcite. Omphacite is not stable in the matrix but was replaced by amphibole + quartz (Fig. 4f). The quartz inclusions in amphibole are sometimes fresh, but more often develop reaction coronas of talc plus calcite (Fig. 4b). Dolomite also contains inclusions of omphacite, magnesite and amphibole and shows a complex chemical zoning with BSE-darker cores and brighter peripheral parts (Figs 4c,g). The degree of brightness increases with Fe-content of dolomite, the source of which, in some cases at least, seems to be inclusions of relict magnesite (Figs 4c,e).

Calcite is modally dominant over magnesite in the matrix, where the former replaces the latter (Fig. 4d) and displays a variety of microstructures, the most common one being non-porous calcite along former grain margins of magnesite and polycrystalline porous calcite towards the centers of such pseudomorphic replacement microstructures (Fig. 5a). However, a non-porous calcite and a mixed type also exist (Figs 5b-d), sometimes with a BSE-zoning due to variable Fe-content, and even a calcite type with complex zoning has been observed

(Figs 5e,f). Finally, a fourth textural type of calcite is filling abundant cracks in dolomite (Fig. 4a). In contrast to sample RPC159, a BSE-bright substance is part of the pseudomorphs. The EDX spectra show predominant Fe and subordinate Si in variable proportions; analytical totals vary largely between 65 and 80 wt%, indicating significant porosity and most likely also the presence of undetected light elements. A tentative identification by Raman spectroscopy points to a combination of goethite + amorphous silica as the most likely constituents. Concentrations of this BSE-bright material often run parallel to former grain boundaries of magnesite between porous and non porous calcite of the pseudomorphs (Figs 4d,g). Xenoblastic magnesite is very often preserved in the centers of such pseudomorphs. Uncorroded magnesite is restricted to inclusions in amphibole and was found in one instance as an inclusion in apatite (Figs 6a-c). Compositional zoning of magnesite and dolomite is due to variable Fe-Mg ratios (see below) and usually rather irregular or patchy and rarely concentric, with more Fe-rich rims.

MINERAL COMPOSITIONS

Quantitative chemical analyses were obtained with a Superprobe JEOL JXA 8200 with 5 WDX spectrometers in the E.F. Stumpfl EMP-Laboratory, Leoben, and additionally with a JEOL JSM 6310 scanning electron microscope equipped with an Oxford Link ISIS EDX spectrometer and a Microspec WDX spectrometer at the University of Graz. Analytical conditions were 15 kV accelerating voltage and 6 nA probe current for silicates and 2 nA for carbonates respectively, with a 1-2µm diameter of the focused beam and counting times were 20-30 seconds on peak and 10-15 seconds on lower and upper background positions respectively. Matrix correction of phi-rho-Z-type was performed with internal software. Standards were adularia (K, Si), garnet (Fe, Mg), rhodonite (Mn), titanite (Ca, Ti), chromite

(Cr), gahnite (Zn) and jadeite (Na), and calcite (Ca), dolomite(Mg) and siderite (Fe, Mn) for carbonate analyses. Mineral formulae and endmembers were calculated with the softwares PET (Dachs, 1998, 2004) and AX (Holland, www.esc.cam.ac.uk/astaff/holland/), and mineral chemical plots with PET or GCDkit (Janousek et al. 2006)

Representative mineral analyses for sample RPC-159 are given in Table 1. Large omphacite grains are slightly zoned, with increasing Na, Al and Fe_{tot} and decreasing Ca and Mg from core to rim (Fig. 7a). The composition range in terms of endmembers is about $Di_{69-75}Hed_2Jd_{15-20}CaTs_3Aeg_{2-5}$. Amphiboles are calcic to sodic-calcic (tremolite to winchite, Figs 7b,c) and display minor compositional zoning in Ca, Mg versus Na, Al, with all other elements remaining constant. Muscovite contains up to 3.40 a.p.f.u. Si, is enriched in barium also in its non-decomposed cores (up to 3.4 wt% or 0.68 a.p.f.u.) and contains a few Mol% of paragonite, talc and pyrophyllite endmembers (Tab. 1). No fresh talc could be found in this sample; the analyses in Table 1 are from a rounded talc-rich pseudomorph with radial cracks in omphacite. Most noteworthy is the complete absence of Al and F.

Symplectite along cracks and rims of omphacite consists of Na-rich diopside, pure albite and an amphibole that is significantly more tremolitic than coarse-grained matrix amphibole.

Magnesite without alteration rims of calcite is more magnesian $Mg_{91-93}Fe_{6-7}Ca_1$ and becomes partly more ferroan during replacement: $Mst_{89-90}Sid_{8-9}Cal_1$ (Fig.8a). Matrix calcite is highest in Mg- and Fe-content ($Cal_{94}Mst_{06}Sid_{01}$) – even without integrating dolomite exsolutions (Fig 8b). The non-porous calcite inclusions in omphacite range from entirely pure $CaCO_3$ to $Cal_{97}Mst_{03}$. Calcite replacing magnesite ranges at the high-Mg end of these compositions. In matrix dolomites, Ca correlates negatively with Mg, with a range of $Cal_{48-50}Mst_{47-49}Sid_{2-3}$, whereby (Mg+Mn+Fe) > Ca (Figs 8c,d). The BSE-brighter dolomite grains within a large dolomite crystal are significantly richer in Ca, with (Mg+Mn+Fe) < Ca.

In sample XU-1 (Table 1) the amphiboles show subtle compositional zoning with barroisitic cores and a trend to more tremolite-rich composition towards the rims (Fig. 7b). Within the first centimeter from the eclogite contact there is no significant change in amphibole composition as a function of distance. Omphacite inclusions are virtually pure ternary diopside-hedenbergite-jadeite solid solutions (very low K, Fe^{3+}, ^{IV}Al) and show a considerable spread in jadeite component from 20 to 42 Mol% (Fig. 6a). The highest jadeite content was found in an inclusion in quartz, followed by inclusions in dolomite and amphibole, with the lowest values for inclusions in calcite (Table 1). The magnesite in sample XU-1 has a slightly higher Fe/Mg ratio (less Ca) than that of sample RPC-159 (Fig. 8a), with a composition range of $Mst_{89-92}Sid_{7-11}Cal_{1}$. Porous and non-porous calcites from the pseudomorphs are indistinguishable in terms of major element composition and cover most of the compositional range of pseudomorphic and non-porous calcites of sample RPC-159 with the exception of pure $CaCO_3$ compositions. Fe is slightly above and Mn below the detection limit, Ca and Mg correlate well and range within $Cal_{97-100}Mst_{0-3}$ (Fig. 7b). Matrix dolomites are less ferroan and thus higher in Mg compared to those in sample RPC-159 (Fig. 8c). The conspicuous BSE-zoning of dolomites corresponds to a relatively narrow composition range from pure $Cal_{50}Mst_{50}$ to Mst_{48-49} $Sid_{1-3}Cal_{48-50}$, whereby (Mg+Mn+Fe) > Ca (Fig 8c, d). Mg is inversely correlated with Fe+Mn, while Ca shows no correlation with any of the other cations.

DISCUSSION

Geothermobarometry and reaction history of the magnesite-bearing marbles

234 A petrogenetic grid in the model system CaO-MgO-SiO_2-H_2O-CO_2 (CMSCH) was calculated
235 with THERMOCALC 3.3 (thermodynamic dataset from 22 Nov. 2003) for the P-T range of
236 1.5 – 4.5 GPa and 300 – 900°C to show the reactions that cause significant modal changes
237 (Fig. 9). Adding the components FeO, Al_2O_3 and Na_2O would increase the variance of these
238 equilibria in the natural samples and stabilize the corresponding assemblages over a larger *P-*
239 *T* range. In addition to the polymorphic phase transitions and the dolomite dissociation curve
240 in the upper left corner, the key feature of this diagram is the strongly pressure-dependent
241 degenerate reaction tremolite = diopside + talc, which passes through 4 invariant points. The
242 reactions, emanating from these points towards higher pressures into the UHP field, delimit
243 the stability field of talc in (1) aragonite-dolomite marbles, (2) dolomite-magnesite marbles
244 and (3) rocks with magnesite as the only carbonate mineral. Towards higher temperatures talc
245 breaks down to quartz/coesite + clinopyroxene or enstatite. Only the terminal breakdown
246 reaction of talc, emanating from invariant point (4) applies to ultrabasic compositions, while
247 the others are valid for quartz-saturated rocks.The coloured ellipses in Fig. 9 indicate *P-T*
248 estimates performed by prior workers.
249 We would first like to discuss the metamorphic history of the investigated marbles in this
250 framework and then compare the *P-T* estimates obtainable from them (using
251 THERMOCALC, mode average*PT*) with prior *P-T* estimates for these areas.
252
253 The observed mineral microstructures and compositions in sample RPC-159 can be explained
254 as follows: an aragonite-bearing dolomite marble passes into the omphacite + talc stability
255 field along the prograde subduction path, and subsequently crosses the dolomite
256 decomposition curve to become an aragonite-magnesite marble. During exhumation,
257 magnesite and aragonite mostly back-react to dolomite, leaving only isolated relics of
258 aragonite (in omphacite, dolomite and matrix) and magnesite (inclusions in dolomite).

During subsequent breakdown of omphacite + talc to amphibole ± quartz all talc is consumed (relics occurring only as rare and poorly preserved inclusions in omphacite and dolomite). Quartz is clearly a reaction product and occurs only as part of this reaction microstructure, generally included in amphibole. Aragonite later transforms to calcite. The coarse-grained omphacite + tremolite assemblage is still largely preserved with the exception of partial symplectite-type retrogression. The fine-grained, porous nature of the minerals pseudomorphically replacing magnesite indicates low temperatures for this stage. The dolomite-in-dolomite microstructure might indicate that at least some magnesite grains were replaced earlier - in a process with different kinetics - by dolomite only.

Omori *et al.* (1999) had already observed the disequilibrium replacement microstructures of magnesite by calcite but not differentiated between the different types of calcite, which makes it possible to better understand the metamorphic evolution. They also observed magnesite being replaced by an inner rim of dolomite and an outer rim of calcite (their Fig. 4b) – a microstructure that was not found in our study but that can be expected and may represent a transitional type to the dolomite-in-dolomite microstructure reported here.

As indicated by the blue ellipses in Fig. 8, Zhang & Liou (1996) derived *P-T* conditions of ca. 760°C and minimum pressures of 2.8 GPa from an eclogite from this area, and Rolfo *et al.* (2004) calculated ca. 730°C and 3.2 GPa as peak conditions recorded by a phengite-bearing eclogite from the area, whereas Schmid (2000) derived maximum *P-T* conditions of ca. 4.2 GPa and 730°C from a phengite-bearing eclogite sampled in the nearby Changpu area. If this rock had actually attained conditions above the dolomite dissociation curve, the composition of magnesite can be used to estimate a minimum pressure from the shift of the reaction curve in the Fe-bearing system. Fe content of dolomite decreases with increasing pressure and was

most likely pure $CaMg(CO_3)_2$ at the breakdown curve. Using the most Fe-rich compositions of magnesite and an ideal solid solution model gives activities of ca. 0.89 for both RPC-159 and XU-1: this would shift the dolomite decomposition reaction to the blue curve labeled $mst_{0.89}$, which is near, but not quite at the *P-T* estimates from eclogites.

These results are very different from what the silicates record, which re-equilibrated during exhumation at pressures of around 2.5 GPa. The position of the amphibole breakdown reaction can shift considerably, depending on actual mineral compositions and the intricacies of the activity models used for amphibole and, to a lesser extent, for clinopyroxene and talc. We used models implemented in the AX software of Holland, which are simplified at least to the degree that fluorine is disregarded. The actual peak metamorphic silicate assemblage stable at conditions estimated from the eclogite samples would have been clinopyroxene + coesite + aragonite + dolomite/magnesite. However, only possible pseudomorphs after former coesite have been found.

Mineral modes, microstructures and compositions of sample XU-1 can be explained in a very similar way as for sample RPC159. The silicates preserve record of retrograde breakdown of omphacite + talc to amphibole ± quartz during decompression, indication of a prior high-pressure if not ultrahigh-pressure history. Omphacite was completely consumed during this reaction, and as talc is a poor container of (U)HP relics, the chance to recover UHP relics is very unlikely in this type of marble. The carbonate microstructures differ from those in RPC159: magnesite was apparently a stable matrix phase during much of the rocks metamorphic history. Magnesite inclusions in apatite indicate that magnesite was most likely present already at the beginning of the metamorphic cycle, and magnesite inclusions in amphibole indicate that it was present as a stable matrix phase during amphibole growth,

309 which occurred at pressures far below the dolomite decomposition curve (Fig. 9). The modal
310 predominance of calcite over magnesite in the thin section seems to be contradictory, but
311 there is no record of primary aragonite. Quite to the contrary, all calcite is of the replacement
312 type, and the very fine grain size of the replacement products as well as the presence of
313 goethite and amorphous silica indicate that this replacement occurred at a very late (cool)
314 stage of the metamorphic history. This would corroborate conclusions drawn by Zhu *et al.*
315 (2009) that the calcite-magnesite replacement microstructures are a product of late-stage Ca-
316 metasomatism. Fe-release from decomposing magnesite at that stage might also explain most
317 of the complex compositional zoning patterns in magnesite and dolomite. The great variety of
318 calcite types indicates that two stages of magnesite replacement may have occurred: an
319 earlier one at higher temperatures producing smooth, non-porous and often compositionally
320 zoned calcite and a later one resulting in porous calcite. It is interesting to note that
321 retrogression of the eclogite also occurs in two main stages, the first one with coarse-grained
322 amphibole and clinozoisite as reaction products, and a second stage of symplectitization.
323 These stages might correlate with the magnesite replacement stages in the adjacent marble
324 and reflect events of fluid pulses passing through. Oscillatory zoned calcites in particular
325 might reflect such fluid activity.
326
327 The earlier metamorphic history of this rock is more difficult to constrain. If it was originally
328 a dolomite-magnesite marble (next to an eclogite), the reactions emanating from invariant
329 point (2) in Fig. 9 apply, and if the *P-T* estimates of Zhu *et al.* (2009) obtained from the
330 eclogite are correct, then this rock must have been outside the stability field of talc, with a
331 clinopyroxene + coesite + dolomite + magnesite peak assemblage. One possible piece of
332 evidence for that may be the only grain of quartz found in the matrix (Fig. 4a), which,
333 embedded in dolomite, may have survived the entire exhumation history. Talc would then

have formed as the first product of back-reaction from coesite and clinopyroxene, and may have also been the first layer separating the coesite-bearing eclogite from the dolomite-magnesite marble. Crossing of the degenerate reaction diopside + talc = tremolite would then have replaced this layer by amphibole and consumed all matrix omphacite in the talc-dominated marble. Quartz inclusions in amphibole start to react with their host during exhumation according to the simplified reaction tremolite + quartz + CO_2 = talc + calcite. The BSE-bright, Fe-rich goethite-SiO_2 material has also been found in this microstructural setting (Fig. 6d-f), indicating that this reaction was coeval with the main stage of matrix magnesite replacement. Fe^{2+} from amphibole (and not from magnesite) may have been the Fe source for goethite in this case.

P-T conditions of ca. 600°C and 3.4-3.7 GPa were derived from an eclogite assemblage from this outcrop and a UHP history is further corroborated by finds of coesite (Zhu *et al.,* 2009). The shift of the dolomite dissociation curve calculated for this sample is again not big enough (Fig. 9) to reach down to the conditions recorded in the eclogite, which could mean that the aragonite + magnesite stability field had not been reached. However, it should be noted that Liu *et al.* (2006) reported inclusions of aragonite and magnesite from within the "UHP-zone" of a zircon, also from the same outcrop, indicating a *P-T* history that is not preserved in the main mineral assemblages of marbles. It is possible that a dolomite-magnesite marble crossed the dolomite dissociation curve, but that all evidence of prior aragonite produced in that field was erased at least in the samples investigated by us.

Interestingly, the composition of matrix dolomites in both samples (Ca<(Mg+Fe+Mn)) indicates that they coexisted with magnesite rather than with aragonite; only the Ca-rich "dolomite-in-dolomite" grains in sample RPC-159 seem to have Ca>(Mg+Fe+Mn). This

359 makes sense for sample XU-1, because all evidence points to a late-stage Ca-introduction into
360 the rock. In fact, these dolomite composition data corroborate the metasomatism hypothesis.
361 In the case of RPC-159, there is no evidence for Ca-transfer into the system, and the amount
362 of high-Mg matrix calcite is definitely higher than the small amount of magnesite relics (ratio
363 of at least 10:1). A possible explanation is that the composition of dolomite growing from
364 aragonite + magnesite is controlled by magnesite rather that aragonite.
365
366 **General implications**
367
368 Impure marbles have not been considered to be particularly useful for high-pressure
369 metamorphic research because most of the reactions known from simple chemical systems
370 like CaO-MgO-SiO_2-H_2O-CO_2 (CMASCH) are mainly temperature-dependent and because
371 rocks with a mixed H_2O-CO_2-fluid are not amenable to constant composition diagrams
372 ("pseudosections"). This is due to the fact that the composition of the fluid, for which the
373 system is inevitably open, changes throughout the metamorphic history in a manner that
374 becomes predictable only by including kinetic boundary conditions.
375
376 Nevertheless we have shown that the degenerate reaction tremolite = diopside + talc is a good
377 barometer that covers a certain *P*-*T* range because all of the minerals involved are solid
378 solutions, and it has played a central role in the *P*-*T* evolution of both samples investigated in
379 this study. As a degenerate reaction it is pertinent for calcite-dolomite, dolomite-magnesite
380 and pure magnesite marbles, with an increasing stability field of clinopyroxene + talc at
381 higher pressures in that sequence. Clinopyroxene-talc-marbles are replaced by clinopyroxene-
382 coesite marbles towards higher *T* and *P*, before the possible onset of dolomite decomposition.
383 The reaction of dolomite = aragonite + magnesite is again highly divariant due to variable Fe-

384 content, mainly in magnesite and dolomite, and is shifted towards lower pressures with
385 increasing Fe, becoming thus amenable for impure marbles in cold subduction zones.
386 Therefore, great care should be taken to not overlook relics of magnesite in “ordinary”
387 calcite-dolomite marbles from UHPM terrains. The role of coesite/quartz and
388 aragonite/calcite “relics” has to be evaluated carefully because both minerals can be reaction
389 products along the retrograde path, too. The role of calcite is even more critical because Mg-
390 free calcite inclusions with radial cracks might be the only criterion to derive a prior
391 aragonite + magnesite stability stage, and calcite can obviously be involved in late-stage
392 disequilibrium replacement reactions and form pseudomorphs that could be misinterpreted as
393 former aragonite.
394
395 The peak assemblage in the diamond stability field is clinopyroxene + coesite + dolomite +
396 aragonite, which is more or less equivalent to clinopyroxene + quartz + dolomite + calcite – a
397 very common assemblage at much lower pressures and higher X_{CO2} in the fluid. Hence it is
398 also vital to search for coesite relics in “normal”-looking marbles from UHP areas.
399
400 Schertl & Okay (1994), Zhang & Liou (1996) and also the results of this study show that
401 dolomite can be good enough as a container to preserve relics such as coesite or magnesite,
402 and even talc that is no longer in equilibrium with matrix clinopyroxene. Hence, massive
403 impure marbles that have not been pervasively infiltrated by fluids during exhumation are
404 considered to preserve high-pressure relics better than metapelites, paragneisses and
405 orthogneisses, and perhaps almost as well as eclogites or metaperidotites. An additional
406 benefit in this respect is the fact that most silicate crystals are separated from each other by
407 the predominant carbonate matrix, so diffusion pathways become longer and silicate minerals
408 which are reaction partners may not come in sufficient contact by diffusion of chemical

species for an actual breakdown reaction to be triggered or run to completion, as in the case of a fluid-consuming reaction.

CONCLUSIONS

Out of two investigated cases of magnesite-bearing impure dolomite-calcite marbles, at least one has in fact attained *P-T* conditions within the magnesite + aragonite stability field. Both the dolomite and the amphibole terminal breakdown reactions are highly useful geobarometers for impure marbles. The microstructures and reaction histories of the carbonate minerals can be quite complex and revelatory. Disequilibrium replacement of magnesite by aragonite/calcite at relatively low temperatures has been observed in both samples and might be common in magnesite-bearing UHP dolomitic marbles. Dolomite has turned out to be a quite useful container for high-pressure relics like magnesite, talc, omphacite or coesite/quartz. Impure calcite-dolomite marbles that have experienced conditions in the aragonite + magnesite stability field during their earlier metamorphic history may be more common than hitherto assumed. This implies *P-T* conditions that lie close to the 5°C/km "geotherm", with corresponding implications for tectonic processes in these orogens.

ACKNOWLEDGEMENTS:

K. Ettinger has been very helpful in optimizing electron microprobe measurements. The first author wants to gratefully acknowledge the financial support for this work by Austrian Science Fund project P22479-N21.

REFERENCES

Buob, A., Luth, R.W., Schmidt, M. & Ulmer, P. (2006): Experiments on $CaCO_3$-$MgCO_3$ solid solutions at high pressure and temperature. *American Mineralogist,* **91,** 435-440.

Dachs, E. (1998): Petrological elementary tools for Mathematica®. *Computers and Geosciences* **24/4,** 219-235.

Dachs, E. (2003):. Petrological elementary tools for Mathematica®; an update. *Computers and Geosciences* **30/2,** 173-182.

Hermann, J. (2003): Carbon recycled into the deep Earth: Evidence from dolomite dissociation in subduction-zone rocks: Comment. *Geology*, **31,** e4-e5.

Janousek, V., Farrow, C.M., Erban, V. (2006): Interpretation of whole-rock geochemical data in igneous geochemistry: introducing Geochemical data Toolkit (GCDkit). *Journal of Petrology* **47/6,** 1255-1259.

Liu, L. & Lin, C. (1995): High-pressure phase transformations of carbonates in the system CaO-MgO-SiO_2-CO_2. *Earth and Planetary Science Letters,* **134,** 297-305.

Liu, F.L., Gerdes, A., Liou, J.G., Xue, H.M. & Liang, F.H. (2006): SHRIMP U-Pb zircon dating from Sulu-Dabie dolomitic marble, eastern China: constraints on prograde, ultrahigh-pressure and retrograde metamorphic ages. *Journal of metamorphic Geology,* **24,** 569-589.

Luth, R.W. (2001): Experimental determination of the reaction aragonite + magnesite = dolomite at 5 to 9 GPa. *Contributions to Mineralogy and Petrology,* **141,** 222-232.

Martinez, I., Zhang, J. & Reeder, R.J. (1996): In situ X-ray diffraction of aragonite and dolomite at high pressure and high temperature: Evidence for dolomite breakdown to aragonite and magnesite. *American Mineralogist,* **81,** 611-624.

Messiga, B., Kienast, J.R., Rebay, G., Riccardi, M.P. & Tribuzio, R., 1999. Cr-rich magnesiochloritoid eclogites from the Monviso ophiolites (Western Alps, Italy). *Journal of metamorphic Geology,* **17,** 287-299.

Morlidge, M., Pawley, A. & Droop, G. (2006): Double carbonate breakdown reactions at high pressures: an experimental study in the system CaO-MgO-FeO-MnO-CO_2. *Contributions to Mineralogy and Petrology,* **152,** 365-373.

Oberhänsli, R., Martinotti, G., Schmid, R. & Liu, X. (2002): Preservation of primary volcanic textures in the ultrahigh-pressure terrain of Dabie Shan. *Geology,* **30,** 699-702.

Omori, S., Liou, J.G., Zhang, R.Y. & Ogasawara, Y. (1998): Petrogenesis of impure dolomitic marble from the Dabie Mountains, central China. *The Island Arc*, **7,** 98-114.

Rolfo, F., Compagnoni, R., Wu, W. & Xu, S. (2004): A coherent lithostratigraphic unit in the coesite-eclogite complex of Dabie Shan, China: geologic and petrologic evidence. *Lithos* **73,** 71-94.

Sato, K. & Katsura, T. (2001): Experimental investigation of dolomite dissociation into aragonite + magnesite up to 8.5 GPa: *Earth and Planetary Science Letters,* **184,** 529-534.

Schertl, H-P. & Okay, A. (1994): Coesite inclusion in dolomite of Dabie Shan, China: petrological and rheological significance. *European Journal of Mineralogy,* **6,** 995-1000.

Schmid, R., Franz, L., Oberhänsli, R & Dong, S. (2000): High-Si phengite, mineral chemistry and P-T evolution of ultrahigh-pressure eclogites and calc-silicates from the Dabie Shan, eastern China. *Geological Journal,* **35,** 183-207.
Schmid, R., Romer, R.L., Franz, L., Oberhänsli, R & Martinotti, G. (2003): Basement-cover sequences within the UHP unit oft he Dabie Shan. *Journal of metamorphic Geology,* **21,** 531-538.

Zhang, L., Ellis, D.J., Arculus, R.J., Jiang, W. & Wie, C. (2003): ‚Forbidden zone' subduction of sediments to 150 km depth – the reaction of dolomite to magnesite + aragonite in the UHPM metapelites from western Tianshan, China. *Journal of metamorphic Geology,* **21**, 523-529.

Zhang, R.Y. & Liou, J.G. (1996): Coesite inclusions in dolomite from eclogite in the southern Dabie mountains, China: the significance of carbonate minerals in the UHPM rocks. *American Mineralogist,* **81,** 181-186.

Zhu, Y-F. & Ogasawara, Y. (2002): Carbon recycled into the deep Earth: Evidence from dolomite dissociation in subduction-zone rocks. *Geology*, **30(10),** 947-950.

Zhu, Y-F. (2003): Carbon recycled into the deep Earth: Evidence from dolomite dissociation in subduction-zone rocks: Reply. *Geology*, **31,** e5-e6.

Zhu, Y-F. (2005): Dolomite decomposition texture in ultrahigh pressure metamorphic marble: new evidence for the deep recycling of crustal material. *Acta Petrologica Sinica,* **21,** 347-354.

Zhu, Y-F., Massonne, H-J., & Zhu, M-F. (2009) : Petrology of low-temperature, ultrahigh-pressure marbles and interlayered coesite-eclogites near Sanqingge, Sulu terrane, eastern China. *Mineralogical Magazine*, **73,** 307-332.

Figure and table captions

Figure 1. The most important reactions defining stability fields in the (ultra)high-pressure regime, with the 5°C/km geotherm for reference.

Figure 2. Sample RPC-159: a) coarse grained matrix omphacite and amphibole in dolomite, with quartz and calcite as early reaction products and later symplectite; b) rare relics of magnesite and talc in dolomite; c) oscillatory-zoned matrix epidote; d) detail of symplectite with fine grained, light grey diopside and coarser-grained tremolite in albite; e) rutile rimmed by retrogression titanite; f) phengitic muscovite in amphibole, decomposing to symplectite of very Ba-rich muscovite, phlogopite and albite; g) pseudomorphs of talc + calcite, possibly after former coesite, with radial cracks in omphacite; h) apatite crystals with oriented monazite exsolutions in a dolomite host.

Figure 2. Sample RPC-159: a-d) magnesite in various stages of replacement by mostly porous calcite and to a minor extent by dolomite and a porous, “talc-like” material (c); e) interstitial calcite with dolomite exsolutions; f) non-porous calcite in omphacite, with radial cracks; g) like (f), but with BSE-brighter relics of aragonite; h) BSE-brighter dolomite-2 within normal matrix dolomite, near magnesite (mostly broken out) and calcite.

Figure 3. Sample XU-1: a) coarse grained matrix amphibole and talc in dolomite, with calcite as crack fillings and pseudomorphs, and a small rounded relic of matrix quartz; b) quartz inclusions in amphibole with reactions rims of calcite + talc; c) strongly zoned dolomite with an inclusion of calcite pseudomorphic after magnesite; d) magnesite with inclusions of dolomite, partly replaced by calcite; note BSE-bright Fe-rich material outlining former grain boundaries; e) detail of (c); f) omphacite relic in matrix dolomite, partly reacted to amphibole + quartz; g) zoned dolomite (detail of d).

Figure 4. Sample XU-1: calcite pseudomorphs after magnesite: a) typically with smooth rim and porous core; b) non-porous; c) non-porous with apparently euhedral magnesite inclusion; d) partly porous, smooth part zoned; e, f) with complex zoning.

Figure 5. Sample XU-1: a) magnesite inclusion in apatite; b, c) magnesite inclusions in amphibole: partly replaced by calcite (b) and fresh (c); d, e) quartz inclusion in amphibole partly replaced by talc, calcite and Fe-rich material; f) like in d) and e), but no quartz visible.

Figure 6. a) Pyroxene classification triangle showing clinopyroxene relics from XU-1 (crosses), omphacite (open circles) and symplectite diopside (dots) from RPC-159; b) Amphibole plots for Si vs. Na on the B-site, and c) Si vs. X_{Mg} for matrix amphiboles from XU-1 (crosses) and RPC-159 (dots).

Figure 7. Carbonates from XU-1 (crosses in all plots) and RPC-159 (other symbols); a) magnesite: fresh or dark parts (circles) and brighter parts (dots); b) calcite: matrix calcite (triangles), replacing magnesite (stars), non-porous calcites (circles) and aragonite (dot); c, d) dolomites: matrix dolomite (circles) and "dolomite-in-dolomite" (dots).

Figure 8. Petrogenetic grid for impure marbles in the system CaO-MgO-SiO_2-H_2O-CO_2. *P-T* conditions constrained in this and prior studies are indicated for sample RPC-159 from Dabieshan (blue) and sample XU-1 from Sulu (red): R = Rolfo *et al.* (2004), S = Schmid *et al.* (2000), ZL = Zhang & Liu (1996) and Z = Zhu *et al.* (2009). The role of the invariant points 1-4 and the pertinent reactions are explained in the text.

Table 1: Representative analyses of silicates and carbonates of samples RPC-159 and XU-1.

Figure 1

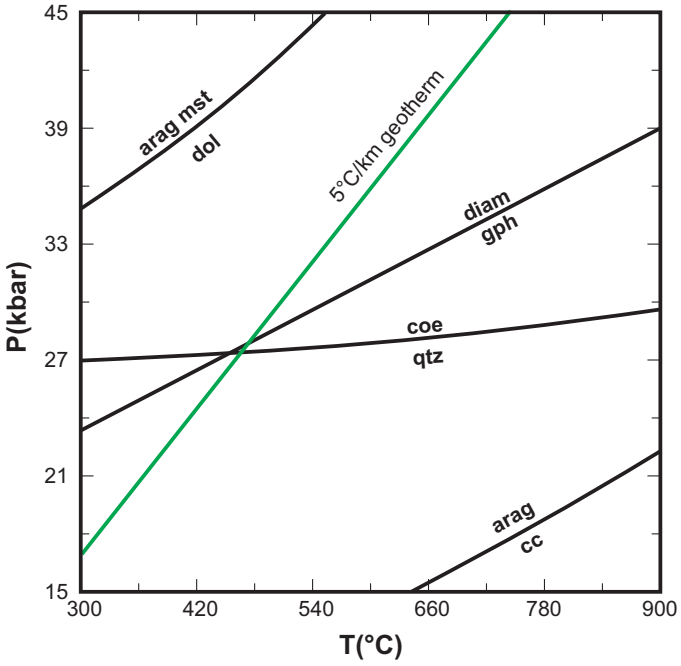
45
39
33
27
21
15
300
420
540
660
780
900
P(kbar)
T(°C)
arag mst
dol
5°C/km geotherm
diam
gph
coe
qtz
arag
cc

Figure 2

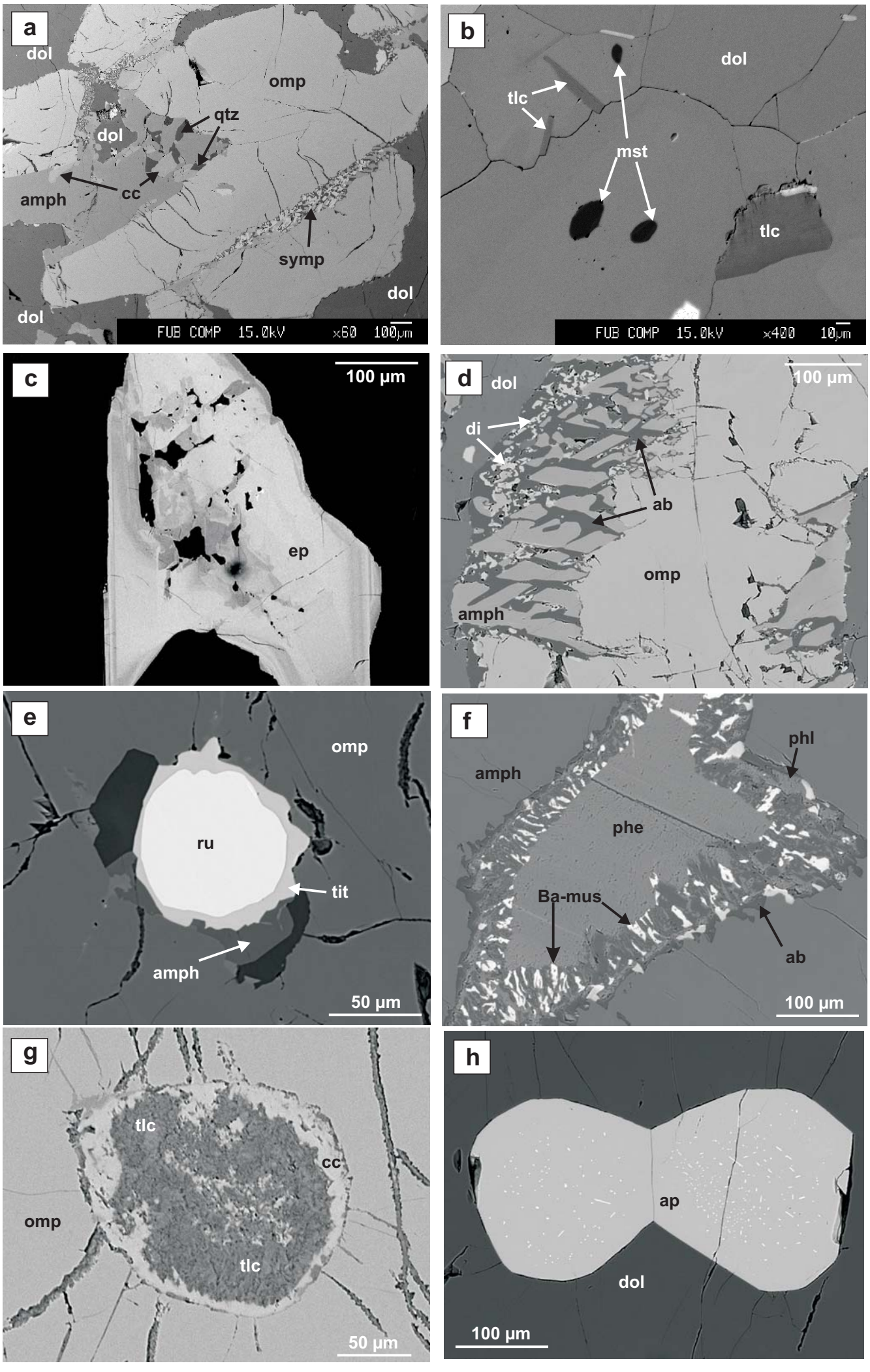
a
dol
omp
qtz
dol
amph
cc
symp
dol
dol
FUB COMP 15.0kV ×60 100µm
b
dol
tlc
mst
tlc
FUB COMP 15.0kV ×400 10µm
c
100 µm
ep
d
dol
100 µm
di
ab
omp
amph
e
omp
ru
tit
amph
50 µm
f
phl
amph
phe
Ba-mus
ab
100 µm
g
tlc
cc
omp
tlc
50 µm
h
ap
dol
100 µm

Figure 3

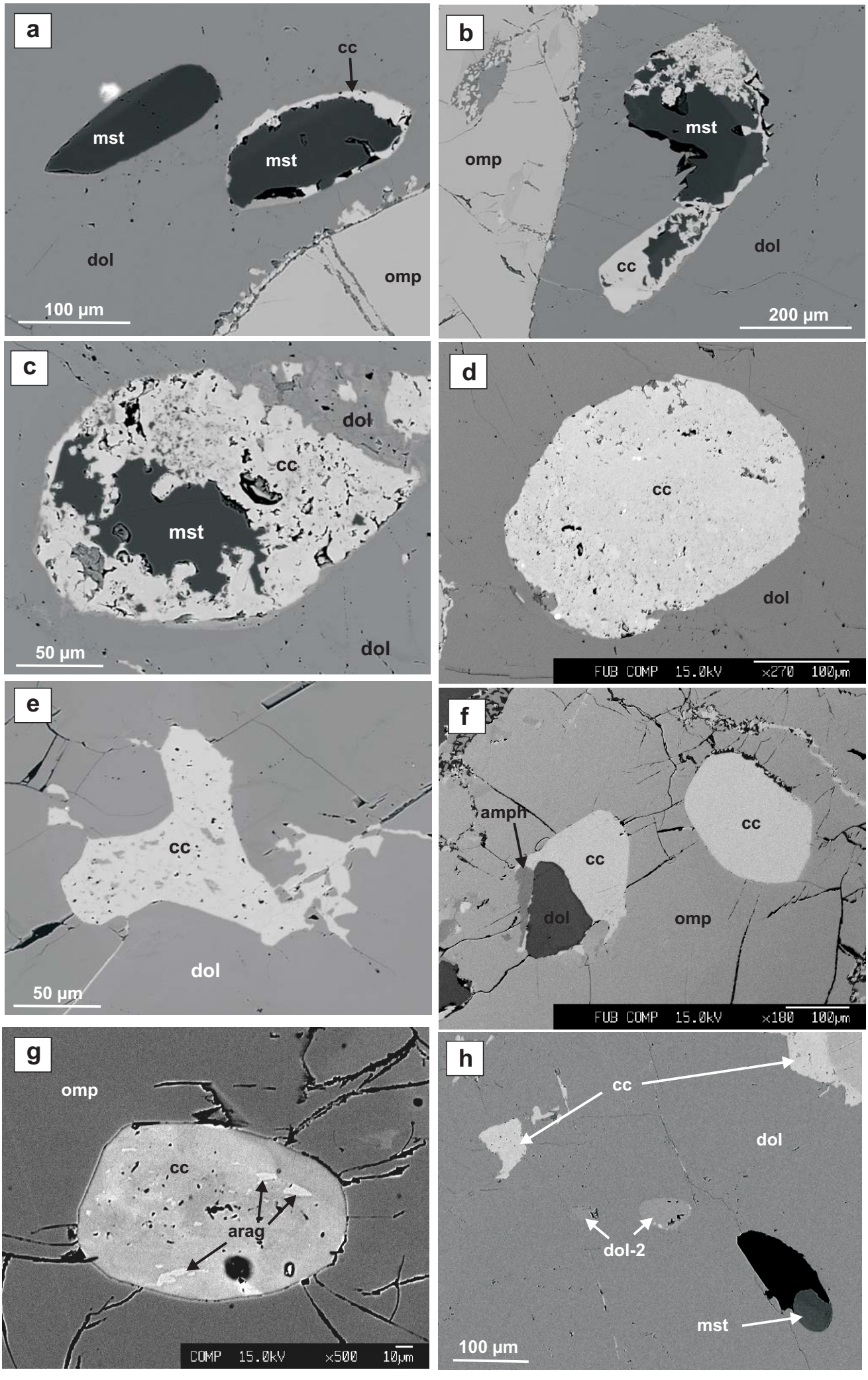
a
cc
mst
mst
dol
omp
100 µm
b
mst
omp
dol
cc
200 µm
c
dol
cc
mst
50 µm
dol
d
cc
dol
FUB COMP 15.0kV ×270 100µm
e
cc
dol
50 µm
f
amph
cc
cc
dol
omp
FUB COMP 15.0kV ×180 100µm
g
omp
cc
arag
COMP 15.0kV ×500 10µm
h
cc
dol
dol-2
mst
100 µm

Figure 4

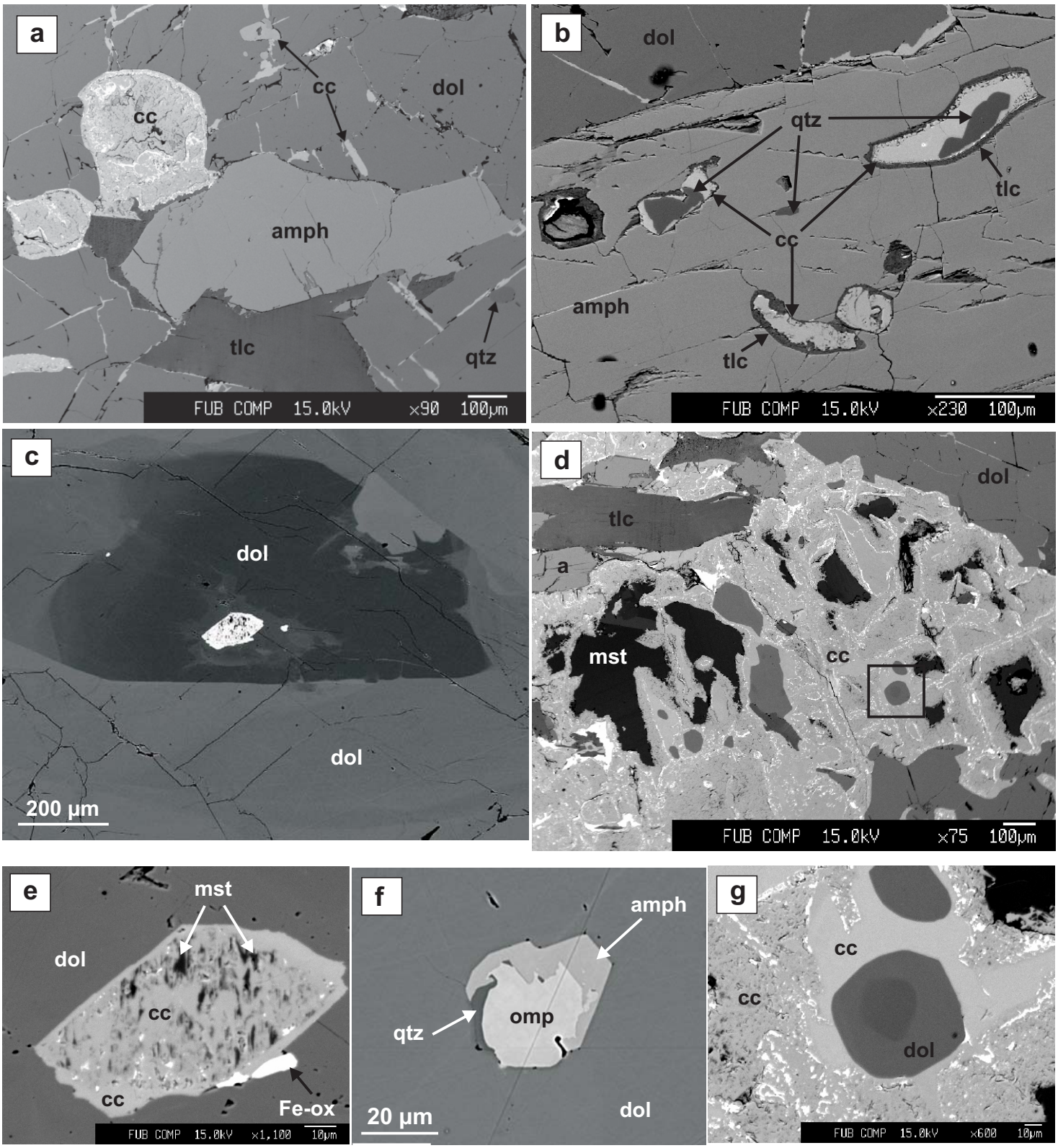
a
cc
dol
cc
amph
tlc
qtz
FUB COMP 15.0kV ×90 100µm
b
dol
qtz
tlc
cc
amph
tlc
FUB COMP 15.0kV ×230 100µm
c
dol
dol
200 µm
d
dol
tlc
a
mst
cc
FUB COMP 15.0kV ×75 100µm
e
mst
dol
cc
cc
Fe-ox
FUB COMP 15.0kV ×1,100 10µm
f
amph
qtz
omp
dol
20 µm
g
cc
cc
dol
FUB COMP 15.0kV ×600 10µm

Figure 5

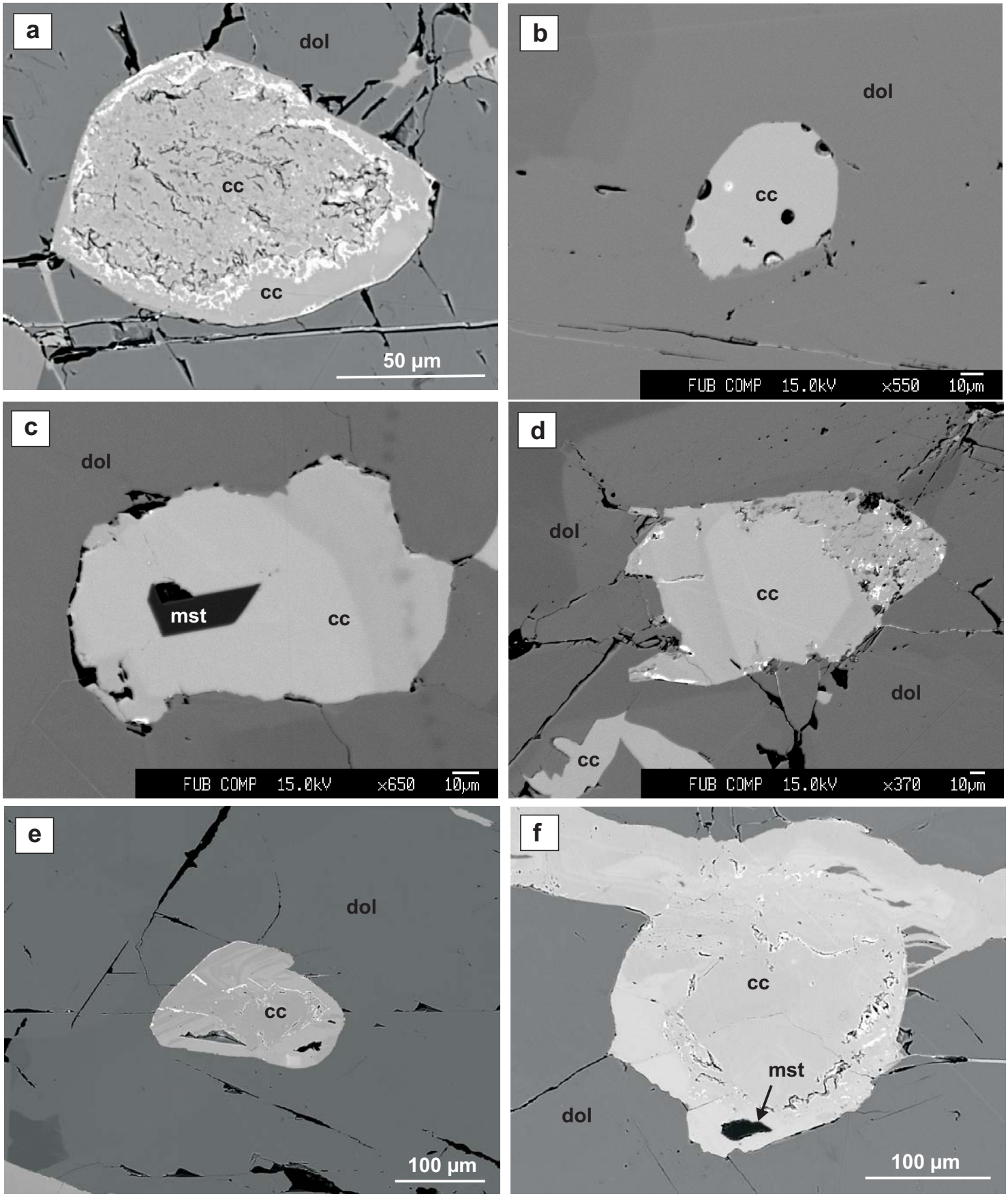
a
dol
cc
cc
50 µm
b
dol
cc
FUB COMP 15.0kV ×550 10µm
c
dol
mst
cc
FUB COMP 15.0kV ×650 10µm
d
dol
cc
dol
cc
FUB COMP 15.0kV ×370 10µm
e
dol
cc
100 µm
f
cc
mst
dol
100 µm

Figure 6

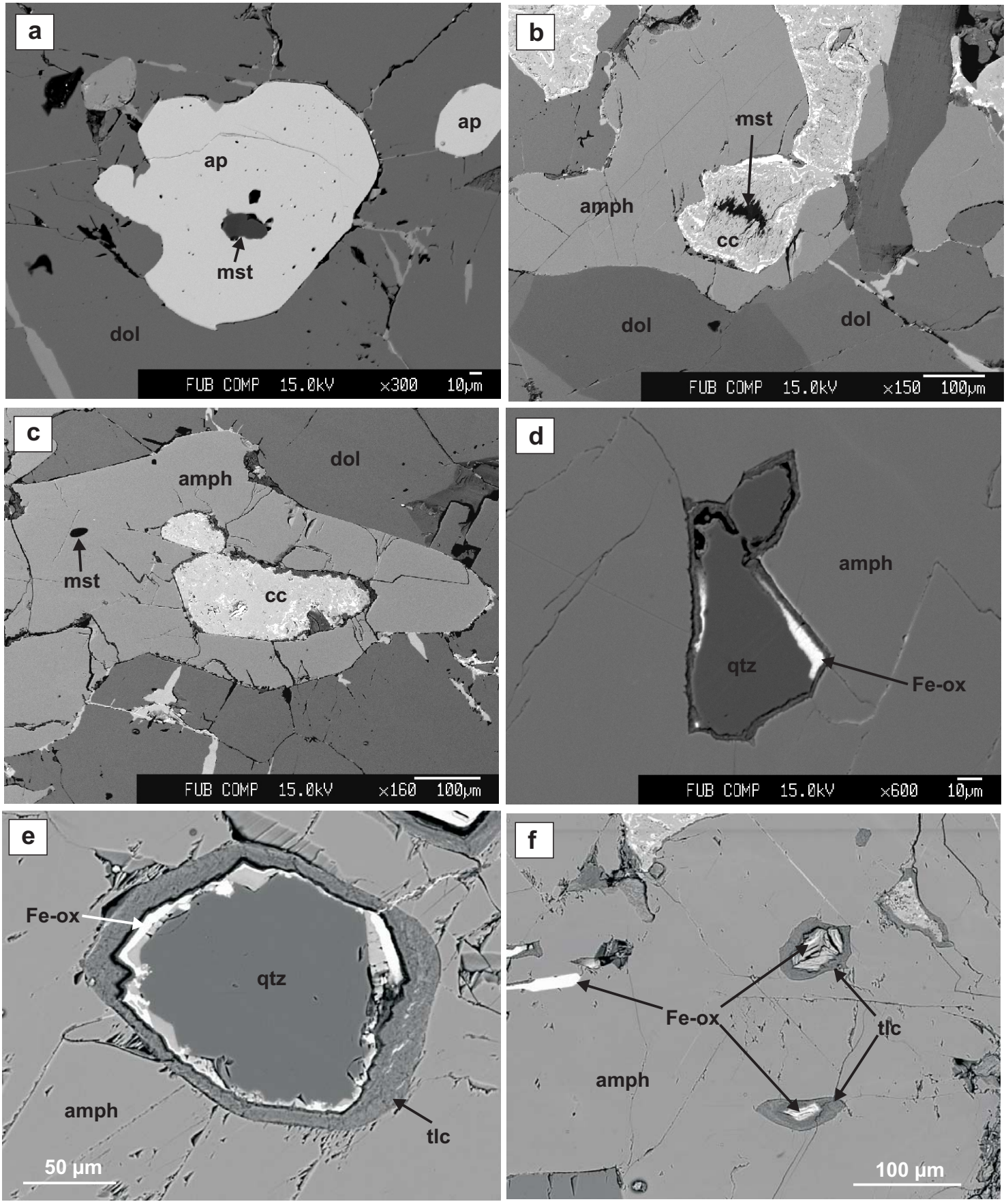
a
ap
ap
mst
dol
FUB COMP 15.0kV ×300 10µm
b
mst
amph
cc
dol
dol
FUB COMP 15.0kV ×150 100µm
c
amph
dol
mst
cc
FUB COMP 15.0kV ×160 100µm
d
amph
qtz
Fe-ox
FUB COMP 15.0kV ×600 10µm
e
Fe-ox
qtz
amph
tlc
50 µm
f
Fe-ox
tlc
amph
100 µm

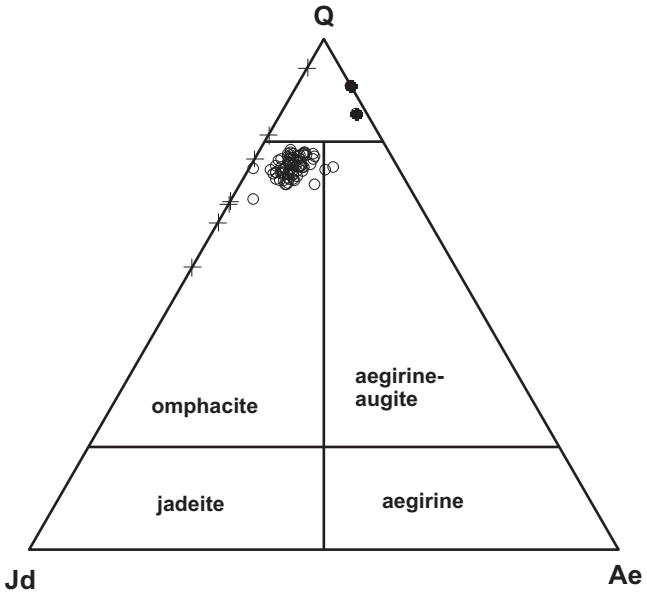

Fig. 7a

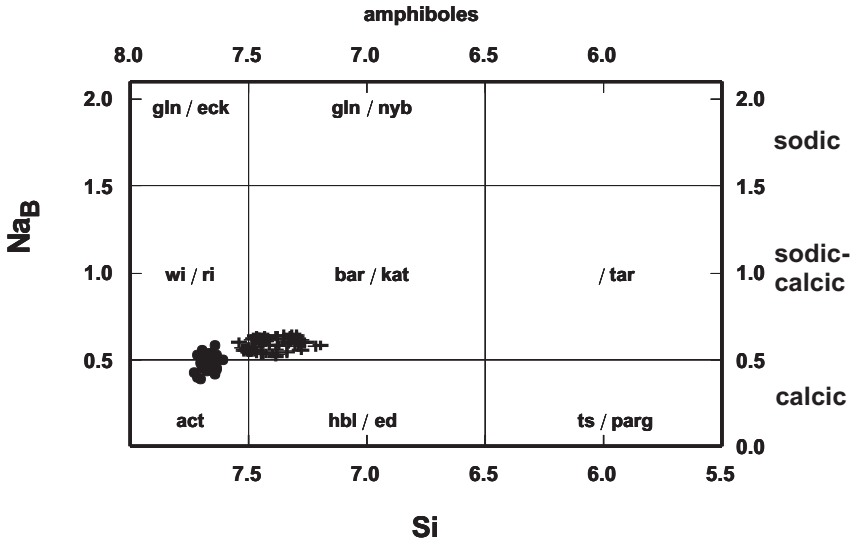

Fig. 7b

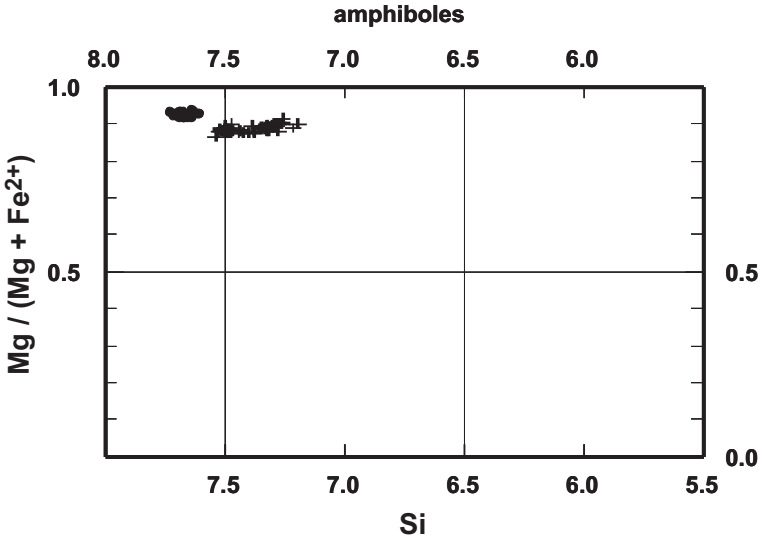

Fig. 7c

Figure 8

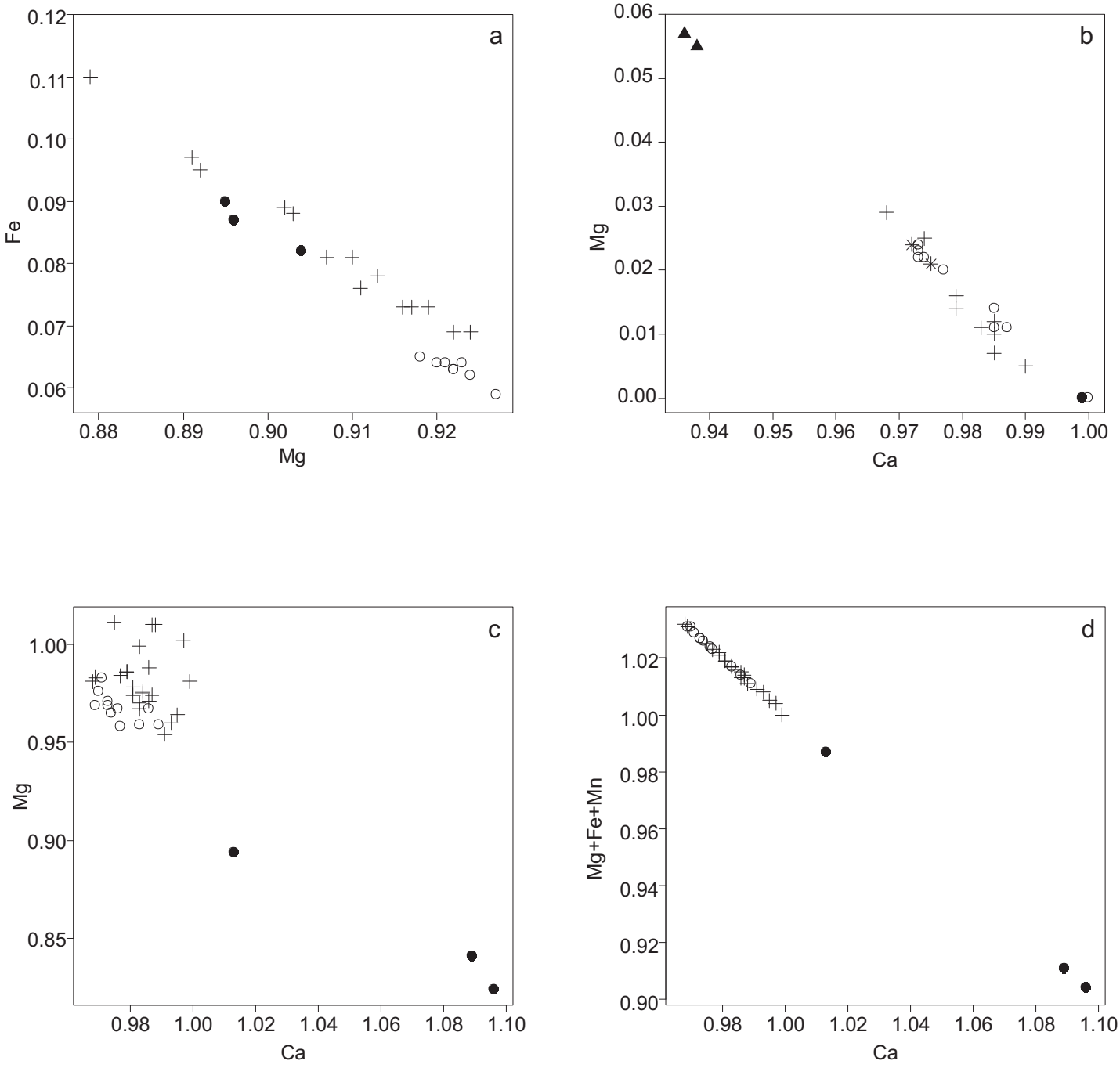
a
Fe
Mg
0.12
0.11
0.10
0.09
0.08
0.07
0.06
0.88
0.89
0.90
0.91
0.92
b
Mg
Ca
0.06
0.05
0.04
0.03
0.02
0.01
0.00
0.94
0.95
0.96
0.97
0.98
0.99
1.00
c
Mg
Ca
1.00
0.95
0.90
0.85
0.98
1.00
1.02
1.04
1.06
1.08
1.10
d
Mg+Fe+Mn
Ca
1.02
1.00
0.98
0.96
0.94
0.92
0.90
0.98
1.00
1.02
1.04
1.06
1.08
1.10

Figure 9

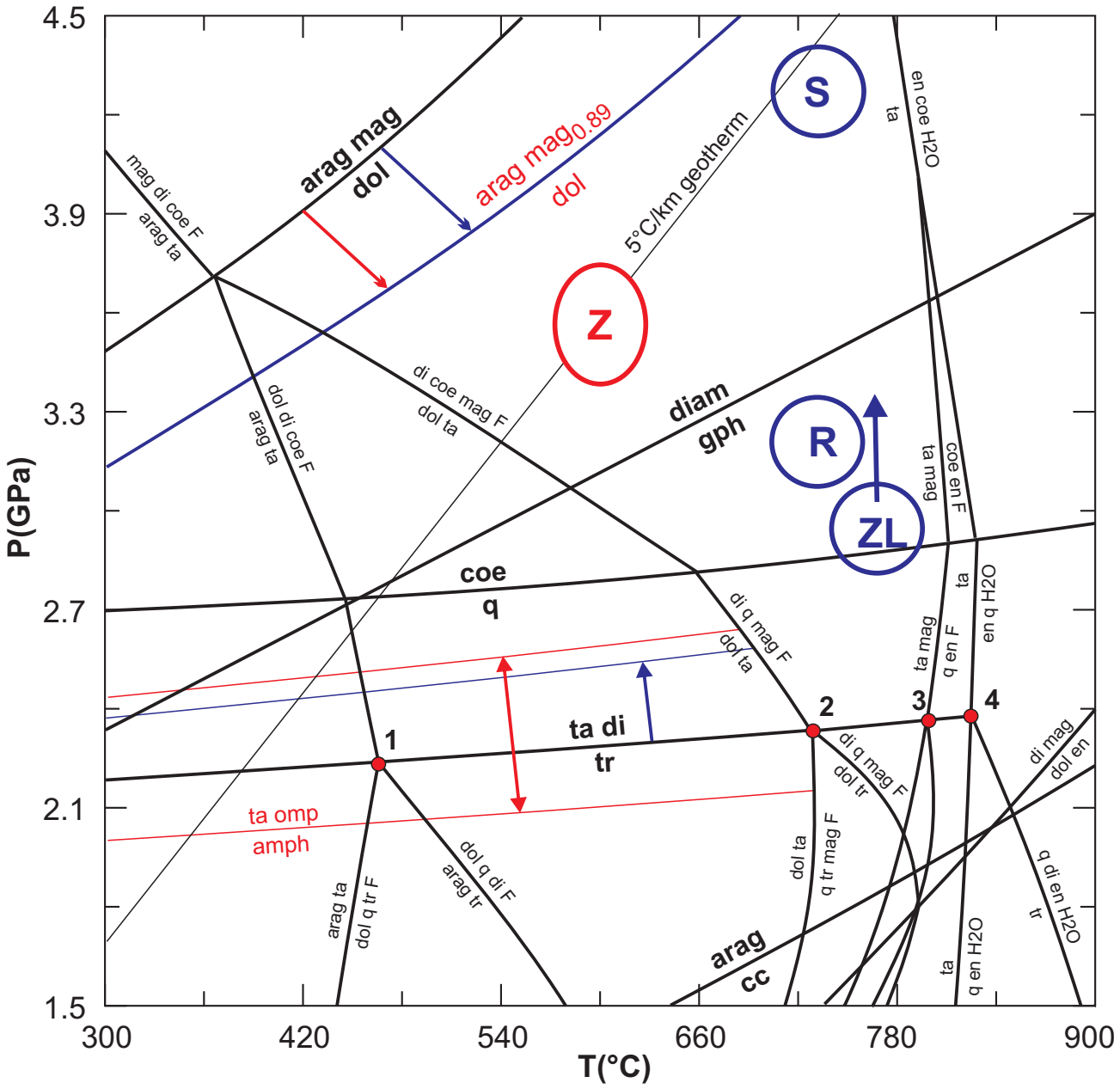
4.5
3.9
3.3
2.7
2.1
1.5
P(GPa)
300
420
540
660
780
900
T(°C)
arag mag
dol
arag mag0.89
dol
5°C/km geotherm
S
Z
R
ZL
mag di coe F
arag ta
dol di coe F
arag ta
di coe mag F
dol ta
diam
gph
coe
q
ta di
tr
ta omp
amph
1
2
3
4
di q mag F
dol ta
dol q di F
arag tr
arag ta
dol q tr F
arag
cc
dol ta
q tr mag F
di q mag F
dol tr
ta
en coe H2O
ta mag
coe en F
ta
en q H2O
ta mag
q en F
ta
q en H2O
di mag
dol en
q di en H2O
tr

	RPC-159									XU-1					
	omp	amph	mus	epidote	cpx	tre	plag	sphene	talc in pseudom.	omp in quartz	omp in dolomite	omp in calcite	talc	amph core	amph rim
SiO_2	55,31	55,32	51,01	38,22	54,31	55,51	67,31	30,44	61,44	57,86	56,91	56,15	63,73	52,16	53,26
TiO_2	0,02	0,06	0,31	0,12	0,00	0,04	0,00	38,66	0,02	0,00	0,00	0,00	0,00	0,09	0,07
Al_2O_3	6,10	5,33	27,23	28,91	1,73	1,93	19,88	1,16	0,09	10,93	8,66	4,46	0,00	8,28	6,51
Cr_2O_3	0,00	0,01	0,00	0,01	0,01	0,00	0,01	0,00	0,00	0,00	0,00	0,00	0,00	0,00	0,01
Fe_2O_3	0,00	0,00	0,00	4,77	0,00	0,00	0,07	0,20	0,00	0,00	0,00	0,00	0,00	0,00	0,00
FeO	1,81	3,08	0,77	0,00	2,72	3,03	0,00	0,00	4,79	2,46	2,43	2,81	1,85	5,25	5,16
MnO	0,00	0,00	0,00	0,02	0,03	0,01	0,00	0,01	0,00	0,00	0,00	0,00	0,00	0,00	0,00
MgO	13,03	20,13	4,71	0,15	15,81	21,74	0,02	0,01	27,93	9,73	11,70	14,27	30,83	17,76	19,16
CaO	19,82	9,82	0,01	24,43	24,22	12,43	0,58	29,70	0,14	14,10	16,18	19,21	0,00	8,86	9,72
BaO	0,00	0,01	3,23	0,00	0,00	0,00	0,00	0,59	0,02	n.a.	n.a.	n.a.	n.a.	n.a.	n.a.
Na_2O	4,02	3,07	0,33	0,01	1,28	1,26	11,77	0,04	0,05	6,21	5,02	3,11	0,00	4,13	3,48
K_2O	0,03	0,21	8,04	0,00	0,00	0,18	0,02	0,00	0,00	0,00	0,00	0,00	0,00	0,31	0,17
F	0,00	0,12	0,00	0,00	0,00	0,06	0,00	0,00	0,00	0,00	0,00	0,00	0,37	0,39	0,19
Cl	0,00	0,01	0,01	0,00	0,00	0,00	0,00	0,00	0,00	n.a.	n.a.	n.a.	n.a.	n.a.	n.a.
Total	100,15	97,18	95,65	96,63	100,11	96,19	99,65	100,81	94,46	101,29	100,90	100,01	96,78	97,23	97,73
Si	1,97	7,63	3,40	2,99	1,96	7,78	2,96	0,99	4,00	2,01	2,00	2,01	4,01	7,30	7,38
Ti	0,00	0,01	0,02	0,01	0,00	0,00	0,00	0,95	0,00	0,00	0,00	0,00	0,00	0,01	0,01
Al	0,26	0,87	2,14	2,67	0,07	0,32	1,03	0,05	0,01	0,45	0,36	0,19	0,00	1,37	1,06
Cr	0,00	0,00	0,00	0,00	0,00	0,00	0,00	0,00	0,00	0,00	0,00	0,00	0,00	0,00	0,00
Fe^{3+}	0,05	0,26	0,00	0,28	0,08	0,00	0,00	0,01	0,00	0,07	0,07	0,08	0,10	0,44	0,27
Fe^{2+}	0,00	0,10	0,04	0,00	0,00	0,35	0,00	0,00	0,26	0,00	0,00	0,00	0,00	0,18	0,33
Mn	0,00	0,00	0,00	0,00	0,00	0,00	0,00	0,00	0,00	0,00	0,00	0,00	0,00	0,00	0,00
Mg	0,69	4,14	0,47	0,02	0,85	4,54	0,00	0,00	2,71	0,50	0,61	0,76	2,89	3,71	3,96
Ca	0,76	1,45	0,00	2,05	0,94	1,87	0,03	1,04	0,01	0,53	0,61	0,74	0,00	1,33	1,44
Ba	0,00	0,00	0,08	0,00	0,00	0,00	0,00	0,01	0,00	0,00	0,00	0,00	0,00	0,00	0,00
Na	0,28	0,82	0,04	0,00	0,09	0,34	1,00	0,00	0,01	0,42	0,34	0,22	0,00	1,12	0,93
K	0,00	0,04	0,68	0,00	0,00	0,03	0,00	0,00	0,00	0,00	0,00	0,00	0,00	0,06	0,03
F	0,00	0,05	0,00	0,00	0,00	0,03	0,00	0,00	0,00	0,00	0,00	0,00	0,07	0,17	0,08
Cl	0,00	0,00	0,00	0,00	0,00	0,00	0,00	0,00	0,00	0,00	0,00	0,00	0,00	0,00	0,00